

ABERRATION CORRECTION IN MICROSCOPES*

W. Wan[#], LBNL, Berkeley, CA 94720, USA

Abstract

Electron microscopes have long been effective tools for scientific research and industrial production. Recently, the success of aberration correction has greatly enhanced the capability of these instruments. This paper attempts to present the basic concept and review the current status of aberration correction in electron microscopes.

INTRODUCTION

The field of electron optics is one of the oldest branches of beam physics, which is the direct descendant of light optics. Recently, it is also one of the most active branches due to the advancement of aberration correction in electron microscopes [1, 2]. In late 2004, a multi-lab project Transmission Aberration-Corrected Electron Microscope (TEAM) was launched to develop the next generation electron microscopes [3]. Initial experiments using the latest aberration corrected Scanning Transmission Electron Microscope (STEM) demonstrated the scientific potential of aberration corrected electron microscopes [4].

Since their invention in the early 30's, electron microscopes have been used in various areas ranging from scientific research to industrial production and different types of microscopes were developed for the specific needs of those applications. The main variations are the transmission electron microscope (TEM), the scanning transmission electron microscope (STEM), the photoemission electron microscope (PEEM), the low energy electron microscope (LEEM) and the scanning electron microscope (SEM). Among them, TEM and STEM are used mainly to study the bulk properties of materials with the electron energy ranges from 100 keV to 1 MeV. PEEM, LEEM and SEM are used to study surface properties of materials with the electron energy below 30 keV. In a PEEM, secondary electrons generated by photons are imaged. In a LEEM, electrons reflected from the sample surface are imaged. In a SEM, an electron probe the size of a few Angstroms is formed on the sample and secondary electrons are collected. Except for LEEM, which needs a magnetic separator to separate the incoming and reflected electron beams, most microscopes without aberration correction are consist of round lenses only. The rotational symmetry of the lenses ensures that the least number of aberrations remain. There are two types of round lenses used in electron microscopes: the electrostatic and the magnetic lenses. The electrostatic lenses are used in PEEMs, LEEMs and some SEMs, whereas the magnetic lenses are used in TEM and STEM where the high voltage prohibits the usage of electrostatic lenses.

*Work supported by the U.S. Department of Energy under Contract No. DE-AC02-05CH11231.

[#]wwan@lbl.gov

Of the remaining aberrations, two are most important in determining the point resolution of a microscope. The first one is the spherical aberration, which is the blurring of the image due to the opening angle of the electron beam at the object. For round lenses, the lowest order spherical aberration is $\Delta r = C_s \alpha^3$, where α is the opening angle.

Figure 1 illustrates the effect of the spherical aberration. The second one is the chromatic aberration, which is due to the combination of the opening angle and the energy spread of the beam. The lowest order chromatic aberration for a round lens is $\Delta r = C_c \alpha \delta$, where $\delta = \Delta E / E$. The effect of the chromatic aberration is illustrated in Fig. 2.

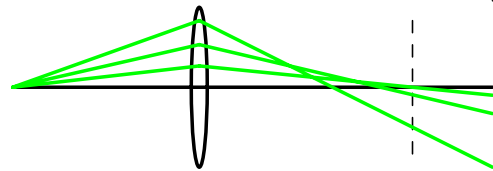


Figure 1: The spherical aberration; the vertical dashed line marks the position of the Gaussian image.

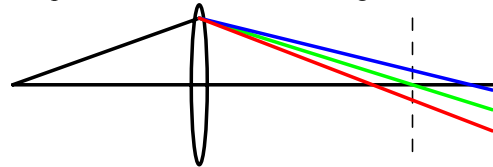


Figure 2: The chromatic aberration; the vertical dashed line marks the position of the Gaussian image; the blue lines represent electrons with higher energy and the red lines represent electrons with lower energy.

Even in the early days of electron microscopes, people contemplated the possibility of correcting the remaining aberrations. Yet the initial result of theoretical investigation is not very encouraging. Scherzer showed that, for a round lens without reflection, the spherical and the chromatic aberrations do not change sign, the same as the focusing power of such a lens [5]. Specifically, electrons with larger angle are focused stronger and electrons with higher energy are focused weaker. As a result, aberration correction requires violation of the above assumptions, through using either multipole elements or electron mirrors. Early attempts on aberration correction, between the late 40's and the early 90's, failed mainly due to technical difficulties. Hence the development of electron microscopes up to the early 90's follows mainly the line of aberration reduction through optimization of the lens design and improvement of stability [6]. The initial success of aberration correction came when the technology was ready in the mid 90's.

In the next two sections, the aberration correction using multipole elements and electron mirrors are described. The former is used in SEM, STEM and TEM and the latter is used in PEEM and LEEM where the low voltage makes the option of electron mirrors feasible. Due to the

limited knowledge of the author and the introductory nature of the paper, the emphasis is on explaining the underlying principle of aberration correction and highlighting key development of aberration correction in electron microscopes. For exhaustive reviews of the subject matter, see ref. [1, 2, 7, 8].

ABERRATION CORRECTION IN SEM/STEM/TEM

The first successful aberration correction was reported in 1995, where the spherical aberration C_S and chromatic aberration C_C were corrected in a low voltage SEM [9]. The corrector consists of four multipole elements (see Fig. 2 and 3), which was originally proposed in the early 60's [10]. Two outer elements are electrostatic multipoles and two inner ones are superimposed electrostatic and magnetic multipoles. As shown in Fig. 3 and 4, the corrector consists of two identical FODO cells with 90 degrees in each plane. Furthermore, it is arranged such that the cosine-like ray of the horizontal plane goes through the center of the left inner element and that of the vertical plane goes through the center of the right inner element. This entails that the knobs correcting $(x|\alpha\delta)$ and $(y|\beta\delta)$ are orthogonal. More importantly, rays in the vertical plane coincide with those in the horizontal plane going backwards. This layout minimizes the breaking of rotational symmetry due to the introduction of multipoles. The most noticeable consequence is that the terms $(x|\alpha\delta)$ and $(y|\beta\delta)$ are equal, restoring the rotational symmetry of the chromatic aberration. The superimposed electrostatic and magnetic quadrupoles form first-order Wien filters that can correct chromatic aberration. In another word, the different energy dependences of the electrostatic and the magnetic forces allow adjusting the chromatic aberration while maintaining overall linear focusing. In addition, the rotational symmetry of the spherical aberration is partially restored. For a rotational symmetric system, we have $(x|\alpha^3) = (x|\alpha\beta^2) = (y|\alpha^2\beta) = (y|\beta^3)$. For the present corrector, the relations among the 4 terms are $(x|\alpha^3) = (y|\beta^3)$ and $(x|\alpha\beta^2) = (y|\alpha^2\beta)$. These relations show that 2 families of octupoles are needed to correct the spherical aberration using a corrector with the same symmetry. For this corrector, the octupole components of the inner multipoles correct the terms $(x|\alpha^3)$ and $(y|\beta^3)$ and those of the outer ones correct $(x|\alpha\beta^2)$ and $(y|\alpha^2\beta)$. With C_S and C_C corrected, the resolution of a 1 keV SEM reached below 2 nm [9].

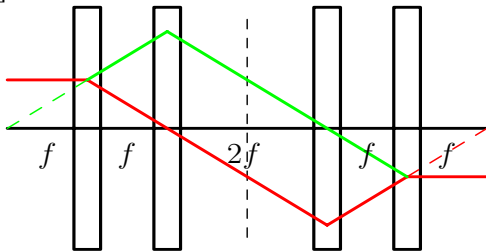


Figure 3: The cosine-like rays of the quadruplet corrector. The red line represents the ray in the horizontal plane and the green line represents the ray in the vertical plane.

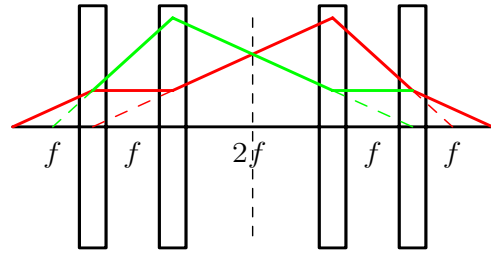


Figure 4: The sine-like rays of the quadruplet corrector. The red line represents the ray in the horizontal plane and the green line represents the ray in the vertical plane.

Meanwhile, Krivanek et. al. successfully corrected third-order spherical aberration in a 100 keV STEM using a quadrupole-octupole corrector [11, 12]. Their second generation corrector uses similar layout for the quadrupoles as the C_S and C_C corrector above, which is shown in Fig. 5 [13]. The linear optics consists of two identical 90 degree FODO cells with equal spacing between the quadrupoles and equal excitation of all quadrupoles. The two outer octupoles correct the terms $(x|\alpha^3)$ and $(y|\beta^3)$ and the middle one corrects $(x|\alpha\beta^2)$ and $(y|\alpha^2\beta)$. Due to the large difference in transverse position of the horizontal and vertical rays in the outer octupoles, the two knobs are largely orthogonal. The resolution of 0.78 Å has been achieved using such a corrector [12].

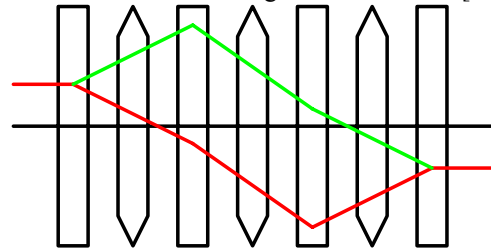


Figure 5: A quadrupole-octupole C_S corrector. The rectangles represent the quadrupoles and the hexagons represent the octupoles. The red line represents the ray in the horizontal plane and the green line represents the ray in the vertical plane.

While the introduction of C_S corrector into an electron microscope corrects the third-order spherical aberration, it also generates much larger fifth-order spherical aberration (C_5) through the combination of the objective lens and the octupoles and that among the octupoles, which becomes the limiting factor as the resolution reach towards 0.5 Å. The equation below illustrates the origin of C_5 through combination.

$$\begin{aligned} \begin{pmatrix} x_f \\ \alpha_f \end{pmatrix} &= \begin{pmatrix} x \\ \alpha + k_{o2}x^3 \end{pmatrix} \circ \begin{pmatrix} R_{11}x + R_{12}\alpha \\ R_{21}x + R_{22}\alpha \end{pmatrix} \circ \begin{pmatrix} x_i \\ \alpha_i + k_{o1}x_i^3 \end{pmatrix} \\ &= \begin{pmatrix} x \\ \alpha + k_{o2}x^3 \end{pmatrix} \circ \begin{pmatrix} R_{11}x_i + R_{12}\alpha_i + R_{12}k_{o1}x_i^3 \\ R_{21}x_i + R_{22}\alpha_i + R_{22}k_{o1}x_i^3 \end{pmatrix} \\ &= \begin{pmatrix} R_{11}x_i + R_{12}\alpha_i + R_{12}k_{o1}x_i^3 \\ R_{21}x_i + R_{22}\alpha_i + R_{22}k_{o1}x_i^3 + k_{o2}(R_{11}x_i + R_{12}\alpha_i + R_{12}k_{o1}x_i^3)^3 \end{pmatrix} \\ &\approx \begin{pmatrix} R_{11}x_i + R_{12}\alpha_i + R_{12}k_{o1}x_i^3 \\ R_{21}x_i + R_{22}\alpha_i + (R_{22}k_{o1} + R_{11}^3k_{o2})x_i^3 + 3R_{11}^2R_{12}k_{o1}k_{o2}x_i^5 \end{pmatrix} \end{aligned}$$

Since C_5 is proportional to R_{12} , it vanishes when R_{12} vanishes, i.e., when the first element is imaged onto the second one [14]. It is obvious from Fig. 5 that this condition is not met for this corrector. More recent designs of C_5 correctors have taken this into account and correct C_5 as well [15, 16]. By adjusting the image location the value of C_5 can be varied and cancelled [17].

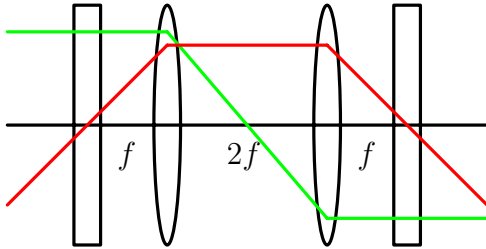


Figure 6: A hexapole C_5 corrector. The ellipses represent the round lenses and the rectangles represent the hexapoles. The red line represents the cosine-like ray in and the green line represents the sine-like ray.

In order to correct C_5 in a TEM, extra attention has to be paid to maintaining large field of view, which usually requires that at least 2000 image points are well resolved in one dimension. It turns out that the simple quadrupole-octupole corrector shown in Fig. 3, 4 and 5 doesn't meet this requirement. The main reason is that the cosine-like ray of the objective lens, i.e. the sine-like ray of the corrector is affected by the octupoles, generating large aberrations limiting the field of view. Although the newest generation of C_5/C_5 has the potential in maintaining large enough field of view [18], the first successful C_5 corrector in a TEM was built based on a different and simpler idea [19, 20, 21]. The corrector consists of two round lenses and two hexapoles, which is shown in Fig. 6. The round lenses forms a $-I$ transport between the centers of the hexapoles, cancelling the second-order aberrations generated by the hexapoles as well C_5 from combination. The third-order spherical aberration can be corrected due to the fact that C_5 from the hexapoles, which is proportional to $(k_s)^2$, is rotationally symmetric and of the opposite sign of that of the round lenses [22].

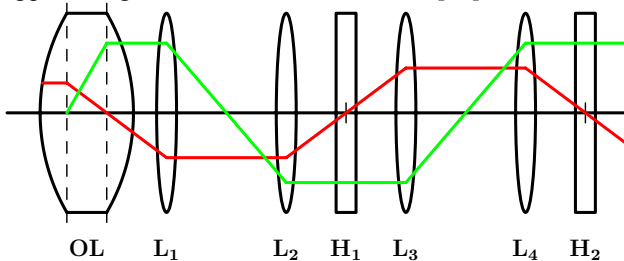


Figure 7: The sine-like (green) and cosine-like (red) rays of a C_5 corrected TEM from the objective lens to the end of the corrector section. The thick lens on the left (OL) is the objective lens. The lenses L_1 to L_4 are round lenses and the rectangles (H_1 and H_2) are hexapoles.

Figure 7 shows such a corrector in a TEM, together with the objective lens and transfer lenses. Note that the cosine-like ray of the objective lens goes through the centers of the hexapoles, hence unaffected by the

corrector, helping to maintain the field of view. A slightly modified version of such a corrector has been used to correct C_5 in STEM [23, 24]. Recently, a STEM named TEAM 0.5 have achieved the resolution of 0.5 Å at 300 keV using such a corrector [25].

With the success of correcting the spherical aberration in TEM, scientists and engineers in this field have set out to build a TEM that is both C_5 and C_C corrected. Successful as it is, the hexapole corrector is not capable of correcting C_C and it is not obvious how to modify the hexapole corrector to include C_C correction. As a result, attention has been focused on the option of a quadrupole-octupole corrector. After many attempts, Rose [7] came up with a design which satisfied the requirement and was later adopted by the TEAM project and built. As shown in Fig. 8, the corrector consists of two multipole quintuplets, each replacing one hexapole in the hexapole corrector.

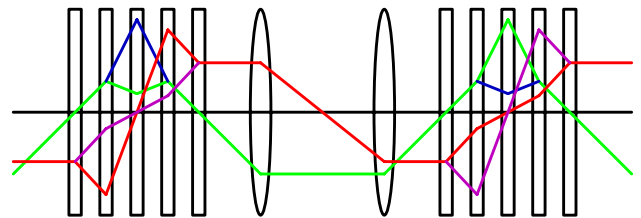


Figure 8: The sine-like and cosine-like rays of the TEAM corrector. The red and green rays are those in the horizontal plane and the blue and magenta rays are those in the vertical plane. The ellipses are round transfer lenses and the rectangles are multipoles. The focal length of the middle elements is half of that of the far outer ones. The ratio of the sine-like rays at the middle elements is 5.

The middle element of each quintuplet is a superimposed electrostatic and magnetic multipole which is responsible for correcting the spherical and the chromatic aberrations. Each quintuplet is mirror symmetric about its center and each half is again mirror symmetric about its own center. Each half of the quintuplet is a FODO cell with 90 phase advance. Or, in the language of optics, it is point to parallel and parallel to point. Each quintuplet is a $-I$ transport. The result is the cancellation of large number of aberrations. Since one out of the two families of the quadrupole components is a free parameter, it is chosen such that the relative difference in the horizontal and vertical beam width at the center of the quintuplet is large. Like the hexapole corrector for TEM, the cosine-like ray of the objective lens is not affected by the aberration corrector (Fig. 9). The second family of octupole can be placed either at the center of the corrector or, as shown in Fig. 9, after the corrector.

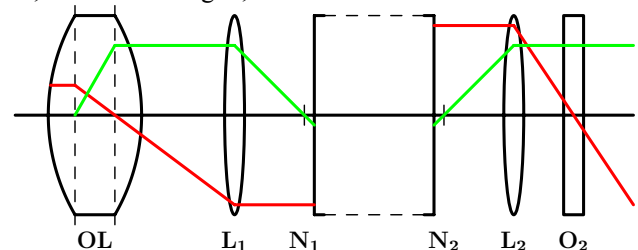


Figure 9: The sine-like (green) and cosine-like (red) rays

of the TEAM microscope from the objective lens to the end of the corrector section. The thick lens on the left (OL) is the objective lens. The omitted part in the middle is the multipole corrector shown in Fig 8. The lenses L_1 and L_2 are adaptor lenses and O_2 is the octupole used to cancel the terms $(x|\alpha\beta^2)$ and $(y|\alpha^2\beta)$.

Such a corrector posed unprecedented challenge on technology in terms of tolerance on alignment errors and power supply ripples. The required tolerance on alignment error is around $14 \mu\text{m}$ between adjacent elements, which is tight but achievable. For the superimposed multipole elements which are responsible for aberration correction, the rms noise level of the current and voltage supplies have to be below $1.5\text{e-}08$ ($\Delta I/I$) and $4\text{e-}08$ ($\Delta U/U$), respectively. This level of stability was unheard of even five years ago. Yet Haider et. al. have recently achieved $\Delta I/I = 8.1\text{e-}09$ and $\Delta U/U = 3.6\text{e-}09$, fulfilling the design criteria [26]. First test of the corrector showed that the resolution of a TEM with this corrector reached 1 \AA [27].

ABERRATION CORRECTION IN PEEM/LEEM

Due to the low energy of the electron beam ($<30 \text{ keV}$), electrostatic lenses are feasible. Although the multipole corrector used in low voltage SEM successfully corrected the spherical and the chromatic aberrations, it is not suited for PEEM or LEEM which requires large field of view. A sophisticated multipole corrector similar to the TEAM corrector may be sufficient but there is a much simpler alternative, which is the electron mirror. The reflection in the mirror makes it possible for a mirror to generate spherical and chromatic aberrations with the opposite sign of those from the regular round lenses [28].

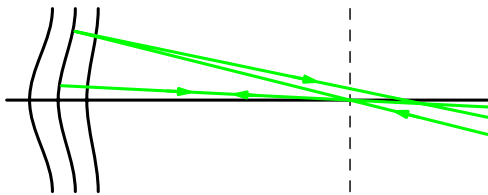


Figure 10: The spherical aberration of an electron mirror showing the possibility of reversing the sign of that of a regular round lens; the vertical dashed line marks the position of the Gaussian image.

As shown in Fig. 10, the electron with large initial angle is reflected at a location where the slope of the field line is smaller than the initial angle and can be focused less. Figure 11 shows that an electron with higher energy penetrates deeper into the mirror, is reflected at a location where the slope of the field line is larger than that for an electron with design energy and, as a result, can be focused more. Therefore, an electron mirror with a dent on the reflection electrode comparable to the electron beam size can form the desired field distribution for aberration correction, one of which is shown in Fig. 12. Four electrodes are used to provide tuning for the focal length, the spherical and the chromatic aberrations.

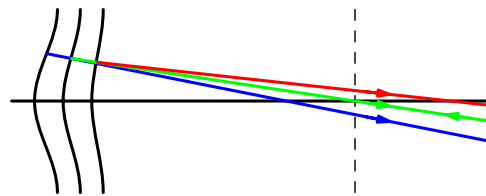


Figure 11: The chromatic aberration of an electron mirror showing the possibility of reversing the sign of that of a regular round lens; the vertical dashed line marks the position of the Gaussian image; the blue lines represent electrons with higher energy and the red lines represent electrons with lower energy.

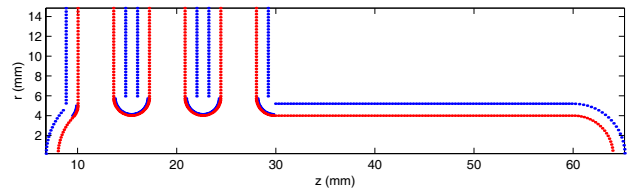


Figure 12: Geometry of the tetrode mirror in PEEM3, which is an adaptation from the SMART design. The red dots follow the surfaces of the electrodes and the blue dots are the locations of the charge rings used for numerical simulation. The first electrode from the right physically ends roughly at $z = 33 \text{ mm}$.

Although the electron mirror itself maintains the rotational symmetry, a magnetic beam separator is needed to guide the electron beam to the detector downstream of the mirror, thus breaking the rotational symmetry of a conventional PEEM (see Fig. 13). Consequently, the most challenging part of an aberration corrected PEEM/LEEM is the beam separator, whose own aberrations have to be small compared to the existing ones. The first aberration corrected PEEM was built at Darmstadt in the 90s and was installed at BESSY II in 2001 [29, 30]. Recently, it achieved the resolution of 3 nm [31]. Its layout is similar to the PEEM in Fig. 13 up to the exit of the beam separator since the design of the later more or less adopted the layout of SMART. There is an energy filter in SAMRT which is absent in Fig. 13. The mirror column forms a $-I$ transport which ensures the cosine-like ray turns back on axis and is unaffected, maintaining a large field of view. The beam separator is a square magnet with 90° bending and 3 axes of mirror symmetry ($\theta = 27.5^\circ, 45^\circ$ and 62.5°) for each pass (see Fig. 14) [31]. The resulting optical system is an achromat with $+I$ transport and free of all second-order geometrical aberrations.

The drawback of this separator is the difficulty in building this device to the tight machining tolerance and in tuning it during operation due to the complexity and rigidity of the design. The fact that focusing is produced primarily by the edges entails that the slope of the grooves and the details of the field near the electron path are critical to the quality of the image. The selection of high μ material to fit the field distribution to the analytical model leads to magnetic material which is soft and hard to machine. Although people on the SMART project succeeded in making such a device, it was by no means trivial. Realizing the difficulty after the engineering

design study [32, 33] and some prototyping, the second project of aberration corrected PEEM, PEEM3 at LBNL, turned to a simpler separator design shown in Fig. 14 [34]. Since the magnet is a simple 90° sector bend, round lenses, with the help of electrostatic quadrupoles provide the focusing. There is only one axis of mirror ($\theta = 45^\circ$) for each pass. The system is a $-I$ transport for each pass with no zero dispersion at the end. An achromat is formed after two passes.

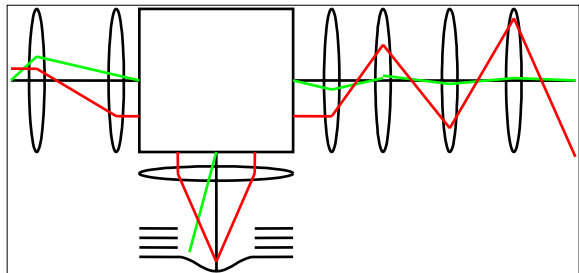


Figure 13: The layout of PEEM3 at LBNL; the square represents the beam separator; the ellipses represent the electrostatic round lenses; the mirror is on the bottom.

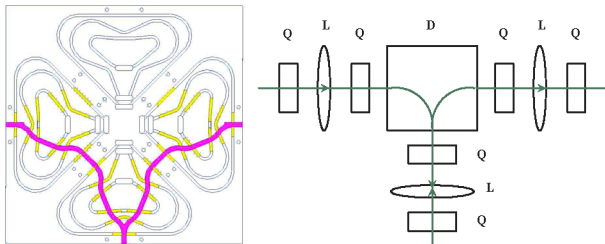


Figure 14: Left: the PEEM3 version of the SMART beam separator. The pink curve is the path of the reference electron. Right: the PEEM3 beam separator. The square is the magnet; the ellipses are the electrostatic round lenses and the rectangles are the electrostatic quadrupoles.

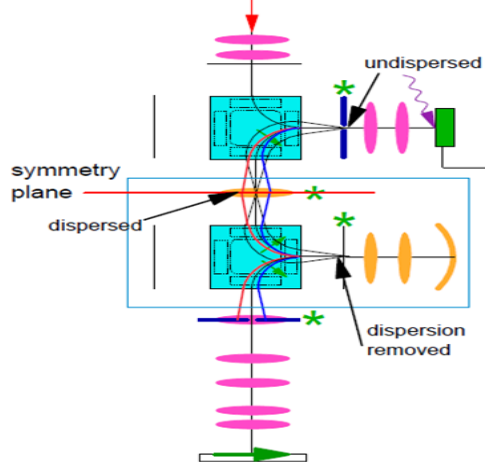


Figure 15: Aberration corrected and energy-filtered LEEM at IBM (courtesy of R. Tromp). The stars mark the locations of the diffraction planes (i.e. where the cosine-like ray crosses the axis); the green arrows in the blue squares and at the end mark the images. The blue squares are the magnetic prisms and the ellipses are electrostatic (orange) or magnetic (pink) round lenses.

Recently, a third aberration corrected PEEM/LEEM has been designed and built at IBM (Fig. 15) [36]. The beam

separator restores the double mirror symmetry of the SMART separator and uses commercially available components. The prism behaves like a round lens to the first order and is mirror symmetric, which entails that the dispersive ray forms a virtual image at the center. As a result, one round lens between the two prisms is sufficient to make the separator an achromat and transfer the image from the center of the first prism to that of the second one. The LEEM has achieved the resolution of 3 nm [37].

REFERENCES

- [1] P. W. Hawkes, "Handbook of Charged Particle Optics" (J. Orlov, Eds., CRC Press, London, 2009), p. 209.
- [2] O. L. Krivanek, "Handbook of Charged Particle Optics" (J. Orlov, Eds., CRC Press, London, 2009), p. 601.
- [3] U. Dahmen, *Microsc. Microanal.* **13** (suppl. 2), 1150 (2007).
- [4] Ç. Ö. Girit *et al.*, *Science* **323**, 1705 (2009).
- [5] O. Scherzer, *Z. Physik* **101**, 593 (1936).
- [6] J. Orlov Eds., "Handbook of Charged Particle Optics" (CRC Press, London, 2009).
- [7] H. Rose, *J. Electron Microsc.* **58**, 77 (2009).
- [8] H. Rose, "Geometrical Charged Particle Optics" (Springer, Heidelberg, 2009).
- [9] J. Zach and M. Haider, *Nucl. Instrum. Methods A* **363**, 316 (1995).
- [10] A. D. Dymnikov and S. Y. Yavor, *Sov. Phys. Tech. Phys.* **8**, 639 (1963).
- [11] P. E. Batson *et al.*, *Nature* **418**, 617 (2002).
- [12] P. D. Nellist *et al.*, *Science* **305**, 1741 (2004).
- [13] O. L. Krivanek, N. Dellby and A. R. Lupini, *Ultramicroscopy* **78**, 1 (1999).
- [14] Z. Shao, *Rev. Sci. Instrum.* **59**, 2429 (1988).
- [15] O. L. Krivanek *et al.*, *Ultramicroscopy* **96**, 229 (2003).
- [16] O. L. Krivanek *et al.*, *Ultramicroscopy* **108**, 179 (2008).
- [17] H. Müller *et al.*, *Phys. Procedia* **1**, 167 (2008).
- [18] N. Dellby, O. L. Krivanek and M. F. Murfitt, *Phys. Procedia* **1**, 179 (2008).
- [19] M. Haider *et al.*, *Ultramicroscopy* **75**, 53 (1998).
- [20] M. Haider *et al.*, *J. Electron Microsc.* **47**, 395 (1998).
- [21] M. Haider *et al.*, *Nature* **392**, 768 (1998).
- [22] P. W. Hawkes, *Philos. Trans. R. Soc. A* **257**, 479 (1965).
- [23] M. Haider, S. Uhlemann and J. Zach, *Ultramicroscopy* **81**, 163 (2000).
- [24] M. Haider *et al.*, *Microsc. Microanal.* **12**, 442 (2006).
- [25] R. Enri *et al.*, *Phys. Rev. Lett.* **102**, 096101 (2009).
- [26] M. Haider *et al.*, *Ultramicroscopy* **108**, 167 (2008).
- [27] B. Kabius *et al.*, *J. Electron Microsc.* **58**, 395 (2009).
- [28] D. Preikszas and H. Rose, *J. Electron Microsc.* **46**, 1 (1997).
- [29] R. Fink *et al.*, *J. Electron Spectrosc.* **84**, 231 (1997).
- [30] Th. Schmidt *et al.*, *Surf. Rev. Lett.* **9**, 223 (2002).
- [31] Th. Schmidt *et al.*, "EMC 2008" (M. Luysberg *et al.*, Eds., Springer-Verlag, Berlin, 2008), p. 7.
- [32] H. Müller, D. Preikszas and H. Rose, *J. Electron Microsc.* **48**, 191 (1999).
- [33] Y. K. Wu *et al.*, *Nucl. Instrum. Methods A* **519**, 230 (2004).
- [34] P. Schmid *et al.*, *Rev. Sci. Instrum.* **76**, 023302 (2005).
- [35] W. Wan, J. Feng and H. A. Padmore, *Nucl. Instrum. Methods A* **564**, 537 (2006).
- [36] R. Tromp, U.S. patent #7,348,566 (2008).
- [37] R. Tromp, private communication.